CHEMISTRY
A EUROPEAN JOURNAL

DOI: 10.1002/chem.200800026

Energy Migration in a Self-Assembled Nonameric Porphyrinic Molecular Box

Lucia Flamigni,*[a] Barbara Ventura,[a] Ana I. Oliva,[b] and Pablo Ballester*[b]

Abstract: We describe the construction of self-assembled double-decker porphyrin arrays built up from two covalently connected trimeric Zn–porphyrin units that are joined together by metal-coordination bonds with diamine ligands. We used three different types of diamine ligands: 1,4-diaza[2.2.2]bicyclooctane (DABCO), 4,4′-bipyridine (BIPY), and 5,15-bis(4-pyridyl)-10,20-diphenylporphyrin (DPYP). The ligands act as pillars, through two axial coordination bonds with the porphyrinic Zn^{II} ions, to block the planes of the porphyrin units in an almost cofacial orientation and inducing the formation of a trigonal prismatic structure. The spectroscopic and photophysical properties of the Zn–trisporphyrin component were determined as well as those of the resulting multimolecular cage-like assemblies. The double-decker assembly with DPYP as the pillars constitutes a nonameric porphyrin aggregate. Although this assembly is thermodynamically less stable than those containing DABCO or BIPY, efficient photoinduced energy transfer occurs (96% yield) from the trisporphyrin base units to the DPYP side walls. The rate of the energy-transfer process is in good agreement with that calculated for a dipole–dipole (Förster) mechanism corrected for the unfavorable orientation geometry of the donor and the axially bound acceptor.

Keywords: energy transfer · photochemistry · porphyrinoids · self-assembly · supramolecular chemistry

Introduction

Elaboration of artificial, noncovalent, multiporphyrin assemblies is important in relation to the mimicry of the biological systems employed for photosynthesis by green plants and purple bacteria. The use of weak forces to assemble complex artificial structures allows, in fact, a closer mimicry of the light-harvesting complexes and the reaction center in the natural photosynthetic apparatus in which the photoactive components are positioned by a protein matrix through a combination of interactions.[1,2] The noncovalent approach is a promising alternative or integration to covalent synthesis and interesting examples of multiporphyrin arrays have been reported.[3] Not all noncovalent artificial multiporphyrinic assemblies that appear in the literature are functional, but they are nevertheless appealing structures due to their inherent beauty.[4] From a practical viewpoint, this type of approach for the production of synthetic structures often has the inconvenience of a low association tendency and poor control over the geometry. This is counterbalanced by the advantage of a simple and fast interchange of components within the system, which does not require the tedious synthesis and difficult purifications of the covalent approach, and makes noncovalent assembly of structures for chemical conversion of light energy a rapidly expanding field.[5]

An effective and widespread strategy for the assembly of noncovalent multicomponent systems based on porphyrins involves axial coordination to the central metal ions of porphyrins by suitable ligands. Examples based on Ru^{II},[6] Co^{II},[7] Rh^{III},[8] Sn^{IV},[9] P^{V},[10] and Al^{III}[11] porphyrins can be found in the literature, but the largest number of reported cases deals with Zn^{II}–porphyrins.[12,13] Pyridines can weakly axially bind to Zn^{II}–porphyrins, with association constants (K_a) in the order of 10^3 to $10^4\,M^{-1}$, depending on pK_a values and steric hindrance on the nitrogen. Such association con-

[a] Dr. L. Flamigni, Dr. B. Ventura
Istituto ISOF-CNR, Via P. Gobetti 101
40129 Bologna (Italy)
Fax: (+39) 051-639-9844
E-mail: flamigni@isof.cnr.it

[b] Dr. A. I. Oliva, Prof. P. Ballester
The Institute of Chemical Research of Catalonia (ICIQ)
and Catalan Institution of Research and Advanced Studies (ICREA)
Avda. Països Catalans 16
43007 Tarragona (Spain)
Fax: (+34) 977-920-221
E-mail: pballester@iciq.es

Supporting information for this article is available on the WWW under http://www.chemeurj.org/ or from the author.

stants cannot provide, at the spectroscopic concentrations used in the photophysical studies, equilibrium mixtures with the assembly as a dominant species. Multiple axial ligations, and when appropriate, close matching of the dimensions are required to achieve the high association constants required for photophysical studies.[5g] For example, bis(Zn–porphyrin) systems with tweezerlike structures and bite angles that match the dimensions of the guest could very effectively complex ($K_a \approx 10^7$–$10^8\,M^{-1}$) photoactive bidentate guests.[13,14] High thermodynamic stability of the multimolecular assemblies has also been obtained with molecules or relatively rigid oligomers with multiple recognition sites in which additive properties have reinforced the interaction between partners, which results in relatively stable photoactive arrays.[15]

Herein, we discuss the formation of thermodynamically stable porphyrin arrays that closely relate to a molecular box. The multimolecular architectures studied herein are roughly trigonal prismatic structures and consist of two covalently connected trimeric Zn–porphyrin units that are joined together by metal-coordination bonds with three diamine ligands. The bidentate ligands 1,4-diaza-[2.2.2]bicyclooctane (DABCO), 4,4′-bipyridine (BIPY) and 5,15-bis(4-pyridyl)-10,20-diphenylporphyrin (DPYP) were used to induce the self-assembly of the molecular box (Scheme 1). Each diamine ligand acts as a pillar, through two axial coordination bonds with the porphyrinic Zn^{II} ions, to block the planes that contain **1** in an almost parallel orientation. The interaction of **1** with each ligand induces the formation of a trigonal prismatic structure of different heights. Assuming a Zn–N bond approximately 2 Å in length, one can anticipate interporphyrin plane distances (i.e., prism heights) of approximately 20, 11.2, and 6.5 Å for the complexes with DPYP, BIPY, and DABCO respectively. Whereas DABCO and BIPY are photochemically "innocent", that is, they do not absorb visible light and will not interact with the excited states of the Zn–porphyrin units, DPYP can interact and is photochemically active under visible light absorption. The spectroscopic and photophysical properties of **1** were determined, as well as those of the resulting multimolecular cagelike assemblies $(DABCO)_3{\cdot}\mathbf{1}_2$, $(BIPY)_3{\cdot}\mathbf{1}_2$, and $(DPYP)_3{\cdot}\mathbf{1}_2$. The DABCO and BIPY assemblies contain photochemically inert pillars that could serve as models for the DPYP assembly, in which a photoinduced energy-transfer process from **1** (base) to the DPYP pillars (side walls) was detected and discussed in the context of current theories.

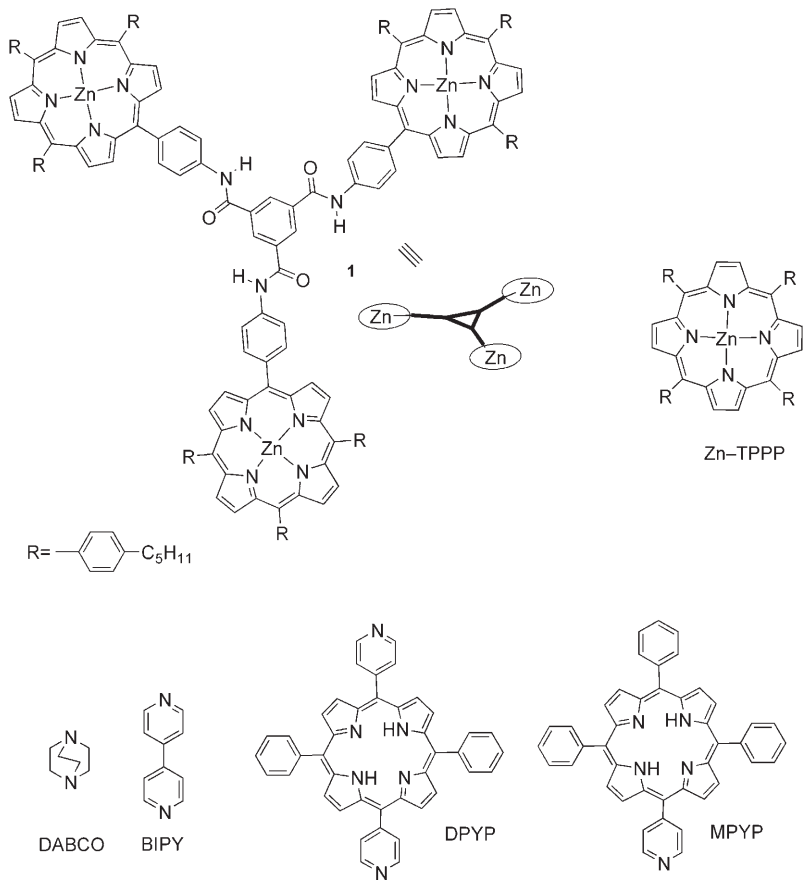

Scheme 1. Structures of the compounds used.

Results and Discussion

Self-assembly: The self-assembly of **1** induced by coordination with DABCO has been previously studied in chloroform and the stability of the 3:2 double-decker molecular cage formed was determined by using a combination of UV-visible absorption and ^{1}H NMR spectroscopic titrations.[16] To study the spectroscopic and photophysical properties of the 3:2 complexes of **1** with DABCO, BIPY, and DPYP, the stability of the corresponding assemblies were evaluated in toluene.

The initial addition of DABCO to a solution of **1** in toluene (porphyrin concentration $\approx 10^{-6}$ M) leads to a shift of the Soret band from 426 to 429 nm (Figure S1 in the Supporting Information). This redshift of the Soret band by 3 nm is characteristic of a 1:2 DABCO·**1** sandwich geometry. The two porphyrin units bound to DABCO are in an almost cofacial arrangement and experience exciton coupling interaction, as shown by the 4 nm blueshift of the corresponding Soret band compared with the same band observed for a

simple Zn–porphyrin axially coordinated to DABCO (433 nm).[17] On addition of more DABCO the intensity of the band at 429 nm decreases and a new band appears at 434 nm. As observed for reference compound Zn–TPPP (TPPP = tetra-*p*-pentylphenylporphyrin), a shift of the Soret absorption band by 8 to 10 nm is typical for the formation of a simple 1:1 DABCO·**1** axial complex. The titration profile is similar to that observed in chloroform, although the shifts in the maximum of the Soret band corresponding to the three species (**1**, the 3:2 complex, and the 3:1 complex) are smaller (the maximum of the Soret band for the three colored species in chloroform appears at 423, 429, and 431 nm, respectively). Another notable difference is the absence of clear isosbestic points when the titration of **1** with DABCO is carried out in toluene instead of chloroform. This observation indicates that the 3:2 assembly starts to dissociate at a DABCO concentration very close to that required for its quantitative formation. Contrary to the observations made in chloroform for the same 3:2 assembly of DABCO and **1**, the cage assembled in toluene is less stable in the presence of excess DABCO.

The titration data obtained in toluene for the interaction of **1** with DABCO were analyzed with regards to the three colored species **1**, the 3:2 assembly, and the 3:1 open complex.[18] Figure 1 shows the formation of these species and

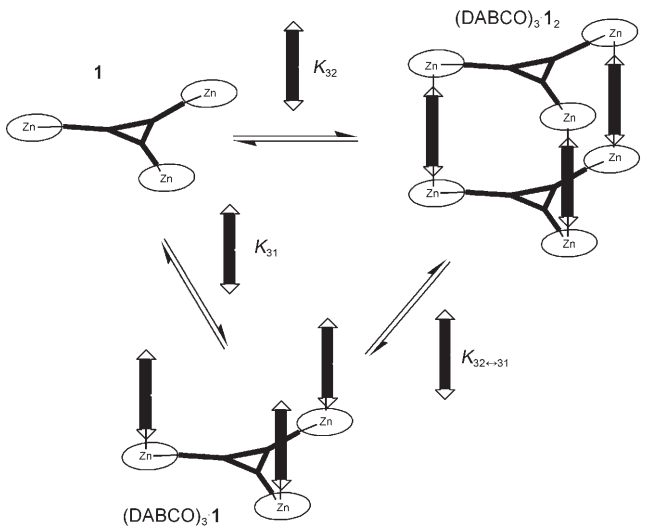

Figure 1. Schematic representation of the species involved in the equilibria for the coordination of DABCO with **1**. The overall equilibrium constants K_{32}, K_{31}, and $K_{32\leftrightarrow 31}$ are also indicated.

the calculated stability constants of the complexes were $K_{31} = 8 \times 10^{14}\,\text{M}^{-3}$ and $K_{32} = 2.5 \times 10^{25}\,\text{M}^{-4}$.[19] Using these stability constant values and the program SPECFIT,[18a] we simulated the speciation profile of **1** (porphyrin concentration $\approx 10^{-6}$ M; Figure 2) with DABCO assuming that **1** is involved exclusively in **1**, $(DABCO)_3$·$\mathbf{1}_2$, and $(DABCO)_3$·**1**. The speciation profiles are very useful to visualize the relative stability of the different multimolecular complexes formed during a self-assembly process. The stability range for each species

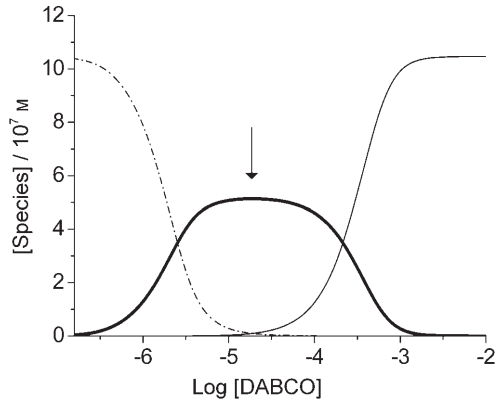

Figure 2. Simulated speciation profile for the titration of **1** with DABCO in toluene ($[\mathbf{1}] = 1 \times 10^{-6}$ M) for **1** (–•–•), $(DABCO)_3$·$\mathbf{1}_2$ (——), and $(DABCO)_3$·**1** (——).

is highly dependent on the concentration at which the assembly process is carried out. We have already mentioned that the values of the stability constants for the 3:2 cage complex and the 3:1 open complex for the DABCO·**1** system in toluene are slightly smaller than those measured in chloroform.[20] The speciation profile shown in Figure 2 indicates that the cage complex, $(DABCO)_3$·$\mathbf{1}_2$, is almost fully assembled in toluene and the concentrations of the other two possible species (**1** and the open 3:1 complex) are negligible at a concentration of 1×10^{-6} M for **1** and 3×10^{-5} M for DABCO. These concentration values were selected to carry out the photophysical and spectroscopic measurements. Note that higher DABCO concentrations do not increase the concentration of the 2:3 assembly, but instead they favor the destruction of the cage.

The self-assembly of **1** into a molecular cage induced by coordination with BIPY was also probed by using UV-visible absorption spectroscopy at micromolar concentrations of **1** (Figure 3). The addition of incremental amounts of BIPY induces the disappearance of the initial Soret band at 426 nm, which corresponds to **1**, and the appearance of a

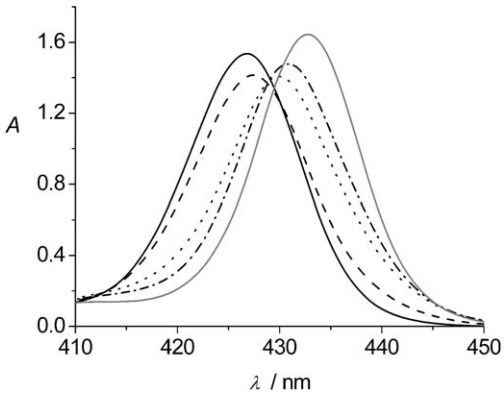

Figure 3. Selected absorption spectra during the course of the titration of **1** with BIPY in toluene ($[\mathbf{1}] = 1 \times 10^{-6}$ M). Spectra were recorded for different amounts of BIPY: 0 (——), 2.1 (-----), 20 (•••••), 803 (–•–•), and 20448 equiv (——).

new band at 430 nm. We assign this 4 nm shift to the formation of the 3:2 BIPY·**1** sandwich complex in which the two porphyrin subunits still experience a weak exciton coupling.[17] On addition of more BIPY, the intensity of the band centered at 430 nm diminishes and a new absorption band appears at 433 nm. We assigned this band to the open $(BIPY)_3$·**1** complex. Again, we did not observe clean isosbestic points during this titration, which is a clear indication that the formation and destruction of the cage occurs in a very similar BIPY concentration range.

The stability constants of the two multimolecular complexes $(BIPY)_3$·$\mathbf{1}_2$ and $(BIPY)_3$·**1** were calculated as described for DABCO, and the values obtained were $K_{31} = 4.7\times10^{11}\,\text{M}^{-3}$ and $K_{32} = 3.2\times10^{21}\,\text{M}^{-4}$ (Table 1). The corresponding simulated speciation profile was also obtained by using SPECFIT software (Figure 4). The photophysical studies were performed at concentrations of 1×10^{-6} M for **1** and 1×10^{-4} M for BIPY to produce the cage as the almost exclusive component of the mixture (see Photophysical properties section).

Table 1. Calculated stability constants (K) in toluene for the self-assembled 3:2 cages and the 3:1 open complexes of **1** with DABCO, BIPY, DPYP, and MPYP. The corresponding microscopic binding constant for the N···Zn interaction is determined for each system. K_m values are also reported.

Pillars	K_{32} [M^{-4}]	K_{31} [M^{-3}]	K_m [M^{-1}]
DABCO	2.5×10^{25}	8×10^{14}	4.6×10^{4}[a]
BIPY	3.2×10^{21}	4.7×10^{11}	3.9×10^{3}[a]
DPYP	2.8×10^{18}	2.5×10^{11}[b]	3.1×10^{3}[c]
MPYP		2.7×10^{10}[d]	3.1×10^{3}[e]

[a] Estimated from $K_m = (K_{31}/8)^{1/3}$. [b] Estimated by using the relationship $K_{31} = 8K_m^3$. [c] Assumed to be equal to that for MPYP. [d] Estimated by using the relationship $K_{31} = K_m^3$ [e] Calculated from ^{1}H NMR spectroscopy titrations (see text for details).

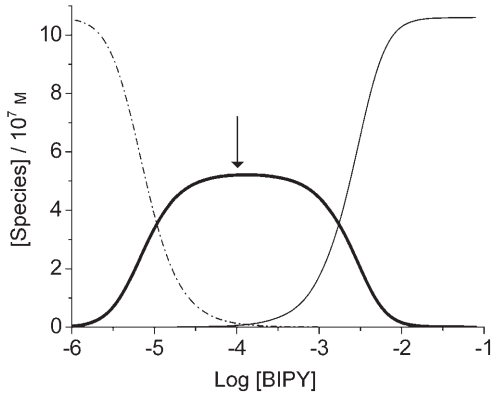

Figure 4. Simulated speciation profile of the titration of **1** with BIPY in toluene ([**1**] = 1×10^{-6} M) for **1** (–•–•), $(BIPY)_3$·$\mathbf{1}_2$ (——), and $(BIPY)_3$·**1** (——).

The experimental study for the calculation of the stability constants of the $(DPYP)_3$·$\mathbf{1}_2$ molecular cage is more complex than for the two previous guests. The minimized structure of this complex is shown in Figure 5. The guest DPYP absorbs in the UV-visible range used to probe the binding process with **1**. In general, it is quite complicated to fit the data of an absorption titration that contains two or more colored species with very similar absorption bands when one of the colored species is found in great excess with respect to the other. This will be the case if we perform a typical titration of **1** with DPYP. To try to overcome this limitation we decided to do the following experiments: First, the optical absorption titration was performed with a constant concentration of **1** = 3×10^{-5} M, which is thirty-fold more concentrated than that typically used for the titrations of **1** with other pyridine derivatives. Second, instead of adding a great excess of DPYP, the titration was stopped when only four equivalents were present in solution. The quantitative assembly of the 3:2 aggregate requires the addition of less equivalents of DPYP when the titration is carried out at higher concentrations of **1**. Moreover, the addition of only four equivalents of DPYP ensures that only the first phase of the binding process, the formation of the 3:2 cage, takes place. The concentration of the open 1:3 complex is negligible over the range of DPYP concentrations used for this titration (see below).

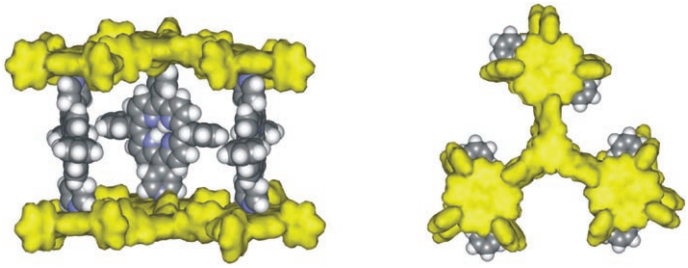

Figure 5. Side (left) and top (right) view of the minimized structure of the trigonal prismatic molecular box formed by coordination of three DPYP components as the pillars and two units of **1** as the bases. DPYP is shown as a CPK representation and **1** is a van der Waals surface model.

Figure 6 shows the Q band region for the titration of **1** with DPYP. The initial addition of DPYP produces a decrease and a small shift in the band centered at 550 nm. The appearance of a shoulder on this band becomes evident on addition of successive amounts of DPYP. The shoulder at 555 nm and the band centered at 515 nm are assigned to the Q bands of DPYP. The titration data were fitted by using SPECFIT software to a binding model that contained only **1**, the 3:2 complex, and DPYP. During the fitting procedure, the absorption spectra of **1** and DPYP were fixed and only the stability constant of the 3:2 complex and its absorption spectrum were used as fitting variables. We obtained a good fit of the titration data to the binding model to give a stability constant of $2.8\times10^{18}\,\text{M}^{-4}$ for the 3:2 complex and a reasonable prediction of its optical absorption spectrum (see Figure S2 in the Supporting Information).

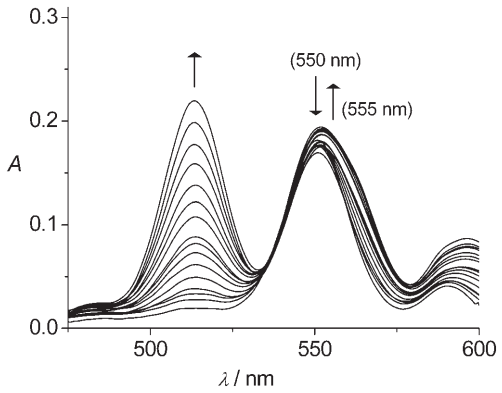

Figure 6. Selected absorption spectra for the titration of trisporphyrin **1** with DPYP in toluene ($[\mathbf{1}]=3\times10^{-5}$ M). Spectra were recorded for different amounts of DPYP: 0, 0.2, 0.4, 0.5, 0.8, 1.1, 1.4, 1.6, 1.8, 2.1, 2.4, 2.7, 3.0, 3.4, 3.8, 4.1 equiv.

In a completely separate experiment, we titrated **1** with MPYP (Scheme 1) and used ^{1}H NMR spectroscopy to determine the microscopic binding for the interaction of **1** with the monodentate ligand. The fit of the titration data to a simple 1:1 binding model taking into account that the concentration of Zn–porphyrin units in solution is three times that of **1** afforded a K_m value of 3.1×10^3 M^{-1}. Using this value, we can estimate the stability constant for the open complex (DPYP)$_3$·**1** from the equation $K_{31}=8\ K_m^3$ to give $K_{31}=2.5\times10^{11}$ M^{-3} (Table 1).

Figure 7 shows the simulated speciation profile for the titration of **1** with DPYP, which we previously performed at

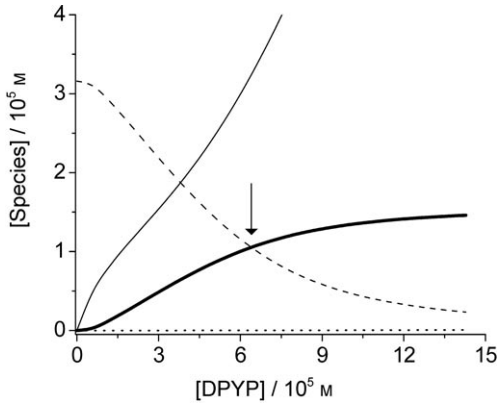

Figure 7. Simulated speciation profile of **1** with DPYP in toluene ($[\mathbf{1}]=3\times10^{-5}$ M) for **1** (-----), DPYP (——), (DPYP)$_3$·**1**$_2$ (——), and (DPYP)$_3$·**1** (•••••).

$[\mathbf{1}]=3\times10^{-5}$ M. The simulated data consider the possible existence of three stoichiometric states of **1**: free **1**, the 3:2 cage complex, and the 3:1 open complex. For the simulation we used the stability constant values determined above for the two assemblies. It can be readily observed that in the DPYP concentration range used, which coincides with the experimental absorption titration described above, the concentration of the 3:1 complex is negligible.

Using the binding model described above and the values determined for the stability constant, we performed several simulations of the speciation profiles at different concentrations of **1** with the goal of finding out the best concentration and stoichiometric ratio to perform the photophysical studies. We wanted to achieve a solution mixture that contained the minimum number of colored species in which the 3:2 cage complex should be present at as high a concentration as possible without necessarily being the major species in solution.

We found that using a concentration of $\mathbf{1}=3\times10^{-5}$ M (Figure 7), the same as that used in the absorption titration, we obtained the best scenario. The cage complex, (DPYP)$_3$·**1**$_2$, coexists with **1**, whereas the concentration of the open complex, (DPYP)$_3$·**1**, is negligible. Looking at the simulated speciation profile at this concentration of **1** it can be readily concluded that both concentrations of these two species, the cage complex and **1**, are 1×10^{-5} M when the concentration of DPYP present in solution is 6.3×10^{-5} M. Consequently, we selected these conditions to perform the photophysical study of the 3:2 cage complex.

Photophysical properties

*Zn–TPPP and **1***: The absorption spectrum of **1** is in good agreement with the simple superposition of the absorption spectrum of the model compound Zn–TPPP when multiplied by a factor of three (see Figure 8). Only a slight red-

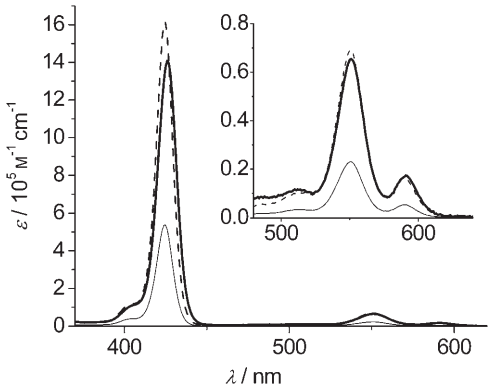

Figure 8. Absorption spectra of **1** (——) and Zn–TPPP (——) in toluene. The absorption of Zn–TPPP multiplied by a factor of three is also shown (-----).

shift (2 nm) and approximately a 10% decrease in the molar absorption coefficient of the Soret band of **1** relative to the sum of the spectra of the component monomers (Figure 8) can be detected, which indicates that there is essentially no electronic coupling between the individual Zn–porphyrin units in **1**.

The luminescence properties of **1** and Zn–TPPP are collected in Table 2; at room temperature almost identical parameters are detected for both. An emission quantum yield (Φ_{fl}) of 0.050, independent of the excitation wavelength, and

Table 2. Luminescence properties and energy levels of the excited states of **1** and Zn–TPPP in toluene.

		295 K			77 K		
	State	λ_{max} [nm]	Φ_{fl}[a]	τ[b] [ns]	λ_{max} [nm]	τ[b] [ns]	E[c] [eV]
Zn–TPPP	^{1}Zn–TPPP	596, 645	0.048	1.9	598, 653	2.4	2.07
	^{3}Zn–TPPP				778		1.59
1	^{1}**1**	596, 645	0.051	1.9	606, 661	2.2	2.04
	^{3}**1**				793		1.56

[a] Fluorescence quantum yields with tetraphenyl porphyrin (TPP) as the standard in aerated toluene (Φ_{fl} = 0.11). Excitation at 560 nm. [b] Excitation at 560 nm. [c] Derived from the emission maxima at 77 K.

Table 3. Luminescence properties and energy levels of the excited states of $(DABCO)_3$·**1**$_2$, $(BIPY)_3$·**1**$_2$, $(DPYP)_3$·**1**$_2$, and DPYP in toluene.

		295 K			77 K		
	State	λ_{max} [nm]	Φ_{fl}[a]	τ[b] [ns]	λ_{max} [nm]	τ[d][ns]	E[f][eV]
$(DABCO)_3$·**1**$_2$	$(DABCO)_3$·^{1}**1**	609, 660	0.051	1.5	642, 701	2.4	1.93
$(BIPY)_3$·**1**$_2$	$(BIPY)_3$·^{1}**1**	609, 661	0.051	1.5	619, 676	2.4	2.00
	$(BIPY)_3$·^{3}**1**				809		1.53
DPYP	^{1}DPYP	647, 712	0.094[b]	9.2[e]	639, 698, 709	14.3	1.94
$(DPYP)_3$·**1**$_2$	$(DPYP)_3$·^{1}**1**$_2$	ca. 606		0.070[d]; 1.9[d,e]	ca. 620	–	2.00
	$(DPYP)_2$(^{1}DPYP)·**1**$_2$	ca. 650, 713	0.056[c]	–; 7.0[e]	ca. 650, 704, 713	12.1	1.91

[a] Fluorescence quantum yields with TPP as the standard in aerated toluene (Φ_{fl} = 0.11). [b] Excitation at 514 nm. [c] Excitation at 660 nm. [d] Excitation at 532 nm. [e] Excitation at 560 nm. [f] Derived from the emission maxima at 77 K.

a lifetime (τ) of 1.9 ns was measured for both compounds. At 77 K in a rigid glass matrix, the fluorescence maxima of **1** shifts to slightly lower energies (606 nm) with respect to Zn–TPPP (598 nm) and the same behavior was observed for the phosphorescence, which is at 778 nm in Zn–TPPP and at 793 nm in **1**. This slight bathochromic shift accounts for a stabilization of approximately 0.03 eV for the singlet and triplet excited states compared with the model.

Cages with DABCO and BIPY: The self-assembled cages induced by the photochemically inert bidentate ligands DABCO and BIPY have been characterized in toluene. Concentrations of 1×10^{-6} M for **1** and 3×10^{-5} M for DABCO were used to form $(DABCO)_3$·**1**$_2$, and concentrations of 1×10^{-6} M for **1** and 1×10^{-4} M for BIPY were used for the cage $(BIPY)_3$·**1**$_2$ (indicated with arrows in Figures 2 and 4). These conditions ensured that the cages were formed as the major species and excluded the presence of **1** or the open complexes in the systems examined. Note that DABCO has no absorption in the range available for the UV-visible determinations, whereas the contribution of BIPY to the spectrum of $(BIPY)_3$·**1**$_2$ appears as a tail on a band extending below 300 nm, so these guests cannot actively participate in the photophysics of the ensemble after excitation with visible light. On the other hand, they cannot act as energy acceptors or electron acceptors, therefore, these complexes are ideal references to display only the effect of complexation on the spectroscopic and photophysical properties of **1**.

A comparison of the spectra of the complexes with the absorption spectrum of **1** multiplied by a factor of two, (see Figure S3 in the Supporting Information) shows that whereas the maximum of the Soret band moves from 426 nm in **1** to 429 nm in the complex with DABCO and to 430 nm in the complex with BIPY, no difference was observed in the Q bands, which in both cases display a shift of 12 nm with respect to **1**.

The luminescence spectra of $(DABCO)_3$·**1**$_2$ and $(BIPY)_3$·**1**$_2$ have maxima at the same wavelengths (Table 3) and display a bathochromic shift of 13 nm with respect to the spectrum of **1**, in agreement with previous reports and with the shift detected in the absorption of the low energy Q bands.[13,21] The fluorescence quantum yield of the two cages is almost identical to that of **1**. The emission spectra of optically matched solutions of Zn–TPPP, **1**, $(DABCO)_3$·**1**$_2$, and $(BIPY)_3$·**1**$_2$ upon excitation at 560 nm are shown in Figure 9. The lifetime

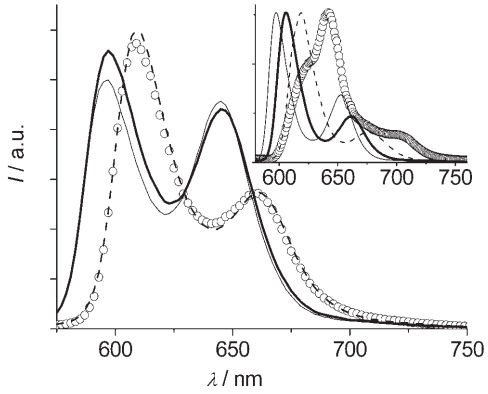

Figure 9. Uncorrected emission spectra of optically matched solutions of Zn–TPPP (——), **1** (——), $(DABCO)_3$·**1**$_2$ (○), and $(BIPY)_3$·**1**$_2$ (-----) in toluene at room temperature for excitation at 560 nm. The inset shows the luminescence data in toluene glass at 77 K.

of both of the cages at room temperature is 1.5 ns, which is approximately 20% shorter than the lifetime of Zn–TPPP (1.9 ns) and in agreement with other reports of Zn–porphyrin complexes with pyridyl residues,[13c,22] whereas at 77 K the lifetime is essentially the same within experimental error. The fluorescence band of $(DABCO)_3$·**1**$_2$ at 77 K is significantly shifted to lower energies with respect to **1** (ca. 900 cm^{-1}) and displays a peculiar spectrum with a shoulder at around 620 nm (Figure 9, inset), which could be explained either by release of **1** from the cage or by a change in the self-assembly mode. The remarkable bathochromic shift in the fluorescence maximum in the glass, could be either due to high stabilization of the excited state of complexed **1** in the rigid media, or to destabilization of the ground-state

energy level, but there are no clues to assess this point. A weak phosphorescence at 809 nm is detected from $(BIPY)_3\cdot\mathbf{1}_2$, whereas no phosphorescence from $(DABCO)_3\cdot\mathbf{1}_2$ can be monitored. It is very likely that a triplet-state stabilization in the complex, similar to that detected for the singlet excited state, would shift the phosphorescence emission to even longer wavelengths. This would increase the nonradiative decay paths that result in essentially no phosphorescence from the $(DABCO)_3\cdot\mathbf{1}_2$ cage.

Cages with DPYP: The stability constant for the assembly of **1** and DPYP is lower than those for the assembly between **1** and DABCO or BIPY, and at spectroscopic concentrations $(DPYP)_3\cdot\mathbf{1}_2$ is present in solution with both **1** and free-base guest DPYP; all strongly absorbing in the spectral region of interest. This fact has to be taken into account in the following discussion.

The assembly of the cage with the photoactive guest DPYP introduces, in addition to the changes in the spectroscopic properties of **1** induced by complexation, alterations in the luminescence properties of both host and guest due to photoinduced processes that can take place within the partners. As far as the former changes are concerned, they will resemble those already reported and discussed above for the assemblies with DABCO and BIPY, therefore, the $(BIPY)_3\cdot\mathbf{1}_2$ complex will be used as a reference model in this aspect owing to the closer similarity between the dimensions of BIPY and DPYP. The spectroscopic properties of free-base DPYP within the assembly, as shown for previous systems, should only be slightly affected.[13c–e]

The absorption spectrum of DPYP (Figure S4 in the Supporting Information) and the luminescence properties listed in Table 3 are in accordance with previously reported data for *trans*-dipyridyl free-base porphyrins.[13c–e] It has a luminescence quantum yield slightly lower than the corresponding tetraphenyl porphyrin (TPP) and a lifetime of 9.2 ns, which increases to 14.3 ns in toluene glass at 77 K.

The cage complex, $(DPYP)_3\cdot\mathbf{1}_2$, is formed following the results of the simulated speciation profile by using concentrations of 3×10^{-5} M for **1** and 6.3×10^{-5} M for DPYP, as indicated by an arrow on the graph in Figure 7. Under these conditions **1** and $(DPYP)_3\cdot\mathbf{1}_2$ are at the same concentration (10^{-5} M) and the concentration of DPYP is 3.3×10^{-5} M. The amount of open 3:1 complex under these conditions is negligible and can be ignored in the spectroscopic analysis of the system. The absorption of the mixture over a 5 mm optical path in the Q band region of the solution is shown in Figure 10. The spectrum contains the contribution of **1** and DPYP involved in $(DPYP)_3\cdot\mathbf{1}_2$ together with the contributions of **1** and DPYP. Figure 10 also shows the absorbance of DPYP (3.3×10^{-5} M) and **1** (10^{-5} M), according to the concentrations of the simulation shown in Figure 7. By subtracting the spectra for DPYP and **1** from the total absorbance, the absorption spectrum of $(DPYP)_3\cdot\mathbf{1}_2$ can be derived. This is shown in Figure 11 and compared with the absorbance of the other components present in the mixture at the pertinent concentrations, namely **1** (10^{-5} M) and DPYP (3.3×10^{-5} M).

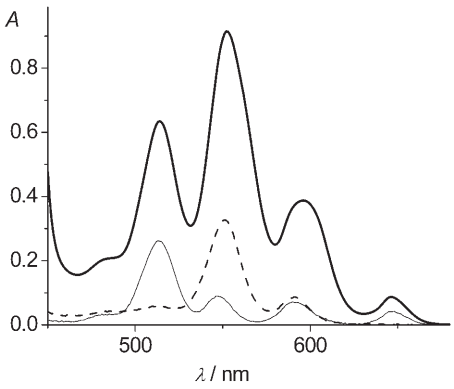

Figure 10. Total absorbance of solutions of **1** (3×10^{-5} M) and DPYP (6.3×10^{-5} M) in toluene (——) and the components **1** (10^{-5} M; -----) and DPYP (3.3×10^{-5} M; ——). Optical path = 5 mm.

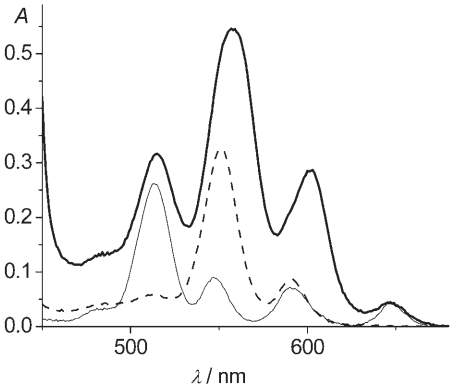

Figure 11. Absorption spectrum of $(DPYP)_3\cdot\mathbf{1}_2$ 10^{-5} M (——) in toluene. The absorption of **1** (-----) and of DPYP (——) present in the mixture is also reported. Optical path 5 mm.

Important information on which component is excited at a selected wavelength can be derived from Figure 11. At wavelengths greater than 650 nm it is possible to selectively excite DPYP, whereas at $\lambda = 570$ nm the absorbing species is essentially **1** within $(DPYP)_3\cdot\mathbf{1}_2$, which has a spectrum different from that of **1**. Selective excitation of the free-base guest DPYP at 660 nm leads to the detection of a decrease of approximately 20% in the emission intensity of the band centered at 713 nm, which is unique to the DPYP emission. If one takes into account that about half of DPYP is part of the complex, this means a decrease of approximately 40% in the emission yield of this chromophore when it is within the complex. This is somehow in contrast with previous studies that report essentially no change in the spectroscopic and photophysical properties of the free-base porphyrin when it is in a double axial coordination through pyridyl residues to Zn^{II}–porphyrins.[13c–e] The decrease is likely to be a result of perturbation of the radiative parameters of DPYP caused by the vicinity of the other DPYP units within the complex or by interaction with **1**.

Excitation of the mixture at 570 nm, a wavelength at which most of the light (ca. 80%, see Figures 10 and 11) is

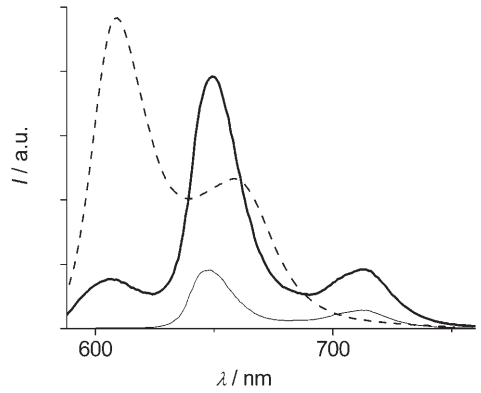

Figure 12. Luminescence of a solution of **1** (3×10^{-5} M) and DPYP (6.3×10^{-5} M) in toluene (——), excited at 570 nm. The emission from the Zn–porphyrin component, obtained by addition of the emission from solutions of models $(BIPY)_3$·**1**$_2$ 10^{-5} M and **1** 10^{-5} M (-----), and the emission of DPYP 6.3×10^{-5} M toluene solutions (——) upon excitation at 570 nm are also reported.

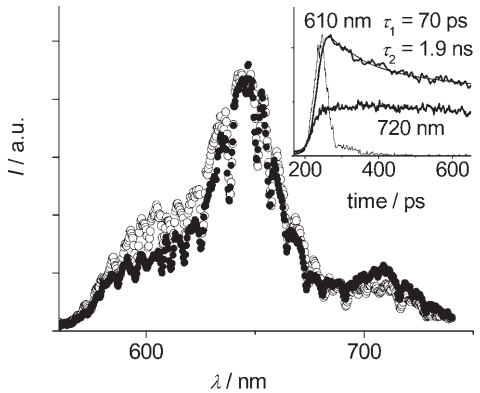

Figure 13. Time-resolved spectra 30 (○) and 300 ps (●) after the pulse of a solution of **1** (3×10^{-5} M) and DPYP (6.3×10^{-5} M) in toluene. The inset shows the time evolution at two selected wavelengths. Excitation at 532 nm, 2 mJ per pulse.

absorbed by the Zn–trisporphyrin unit in the complex leads to the emission spectrum shown in Figure 12. Figure 12 also shows the luminescence spectra from the Zn–porphyrin component (obtained by adding the emission from the model complex $(BIPY)_3$·**1**$_2$ at 10^{-5} M and the emission from **1** at 10^{-5} M) and the luminescence from the free-base component DPYP at 6.3×10^{-5} M. The results can be interpreted as follows: the luminescence of **1** (λ_{max} around 600–620 nm) is clearly quenched compared with the emission from the model compounds since this band is considerably reduced. Considering that excitation at 570 nm leads to the excitation of a small percentage of freely dispersed **1** (ca. 15%; see Figure 11) the residual emission observed at around 600 nm can be attributed to it, which indicates that the emission of **1** involved in the cage is completely quenched. On the contrary, the band at 713 nm, typical of the DPYP emission, is enhanced with respect to the model free-base. This indicates that the luminescence of DPYP is sensitized upon energy transfer from the Zn–porphyrin component and this, given the short lifetime of the Zn–porphyrin excited state, can only occur within the complex.

Time-resolved experiments on a nanosecond timescale performed on the same solution (**1** (3×10^{-5} M) and DPYP (6.3×10^{-5} M)) indicated a lifetime of 1.9 ns for the emission at 600 nm and a biexponential decay, with lifetimes of 7.0 and 9.2 ns, for the emission centered at 713 nm. The first lifetime is coincident with that of **1** and can be clearly assigned to uncomplexed **1** (10^{-5} M) present in the solution. As the band at 713 nm arises from the emission of both the complexed and freely dispersed DPYP, the two observed lifetimes can be ascribed to the two forms, which reveals that complexed DPYP has a lifetime (7 ns) that is reduced compared with that of the model (9.2 ns) in agreement with the decrease of the luminescence quantum yield discussed above. Increase of the time resolution to the picosecond range with excitation at 532 nm indicates the existence of a fast process with a decay centered at around 600 nm and a rise around 720 nm. Figure 13 shows the time-resolved spectra 30 ps after the pulse (○) and after a delay of approximately 300 ps (●) and provides evidence for the evolution of the spectrum during this time interval. The profile of the decay at around 600 nm, typical of the Zn–porphyrin emission, has a biexponential evolution that can be fitted with lifetimes of 70 ps and 1.9 ns in a ratio of 1:1 (Figure 13, inset). The 70 ps decay is ascribed to the quenching reaction of **1** within the complex, whereas the longer lifetime is the contribution of **1** dispersed in solution. A small rise with a time compatible with a lifetime of 70 ps can be detected at 720 nm, the wavelength at which the DPYP acceptor emits, but a precise fitting is made difficult by the very small component with a rising signal. Most of the excited population of DPYP is in fact directly formed upon excitation at 532 nm (see Figure 11), which makes the rise a small fraction of the total DPYP singlet excited state.

Photoinduced processes in the complex: The energy-level diagram for the photoactive system $(DPYP)_3$·**1**$_2$ is shown in Figure 14. The energy levels of the lowest singlet excited states involved in the process are derived from the luminescence maxima detected at 77 K (Tables 2 and 3). The energy level of the singlet excited state of the DPYP that is part of the cage appears to be slightly bathochromically shifted with respect to the model DPYP (although the overlap with the emission from the Zn–porphyrin component makes its precise determination difficult), that is, at 1.91 eV rather than at 1.94 eV as in the DPYP. The energy level of the singlet excited state of **1** in the cage is taken from the data for $(BIPY)_3$·**1**$_2$, which is the reference model for complexed **1**, that is, at 2.0 eV. Therefore, there is a driving force for the energy-transfer reaction from the Zn–porphyrin component to the free-base porphyrin component within $(DPYP)_3$·**1**$_2$; the estimated ΔG^0 for the reaction is −0.09 eV. The experimental energy-transfer rate, defined as $k_{en}=1/\tau-1/\tau_0$, in which τ and τ_0 are the lifetimes of the quenched donor unit (i.e., **1** involved in the cage) and the lifetime of the unquenched unit (i.e., the lifetime of the reference model

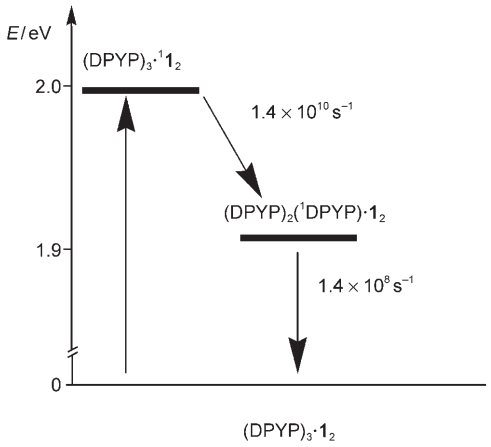

Figure 14. Energy-level diagram for photoinduced energy transfer in $(DPYP)_3$·**1**$_2$.

$(BIPY)_3$·**1**$_2$), respectively, is $1.4\times10^{10}\ s^{-1}$. The efficiency of energy transfer, calculated from $\Phi_{et}=k_{en}/(k_{en}+\tau_0^{-1})$, is very high, in the order of 96%.

We will discuss the energy-transfer experimental rate in terms of the Förster theory, which interprets the process as a dipole–dipole interaction. In general, this is the mechanism that operates when strongly emitting donors and strongly absorbing acceptors (porphyrins) are involved. Within this theory it is possible to calculate, on the basis of geometric, spectroscopic, and photophysical data, the rate constant of the process, k_{en}^F, by means of Equation (1):[23]

$$k_{en}^F=\frac{8.8\times10^{-25}\kappa^2\Phi}{n^4\tau_0 {d_{DA}}^6}J^F \qquad (1)$$

Φ is the emission quantum yield (0.051) and τ_0 is the lifetime (1.5 ns) of donor **1** in the model complex $(BIPY)_3$·**1**$_2$, d_{DA} is the donor–acceptor center-to-center distance (ca. 10 Å), n is the refractive index of toluene, and J^F is the overlap integral calculated from the luminescence spectrum of the donor, $F(\bar{\nu})$, and the absorption spectrum of the acceptor, $\varepsilon(\bar{\nu})$ and has a value of $1.56\times10^{-14}\ cm^3\,M^{-1}$ derived from Equation (2):

$$J_F=\frac{\int F(\bar{\nu})\varepsilon(\bar{\nu})/\bar{\nu}^4 d\bar{\nu}}{\int F(\bar{\nu})d\bar{\nu}} \qquad (2)$$

κ^2 in Equation (1) is the orientation factor and takes into account the relative orientation of the transition dipole moments of the donor and the acceptor. Whereas the value of the orientation factor is statistical (i.e., $^2/_3$) in reacting partners that freely diffuse in solution because they are randomly approaching, the value for κ^2 can be quite different when the two partners are blocked in rigid positions with respect to each other. In this case κ^2 can be calculated from Equation (3):[24]

$$\kappa^2=(\sin\theta_D\sin\theta_A\cos\phi-2\cos\theta_D\cos\theta_A)^2 \qquad (3)$$

in which θ_D and θ_A are the angles formed between the line connecting the donor and acceptor centers and the transition moments of the donor and acceptor, respectively, and ϕ is the angle between the projections of the transition moments on a plane perpendicular to the line connecting the centers of the donor and acceptor. The transition dipole of the Zn–porphyrin donor is degenerate on the plane of the tetrapyrrolic ring and the transition dipole of the free-base porphyrin guest is oriented along the direction of the pyrrolic nitrogen atoms.[13c] In the presence of axial coordination, the planes containing the donor and acceptor porphyrins are perpendicular, θ_D is 90°, and θ_A is 45°, whereas ϕ varies between 0 and 360°. Under these conditions the average κ^2 value is in the order of 0.2. By introducing this value, together with the pertinent parameters, into Equation (2), a rate constant of $k_{en}=1.9\times10^{10}$ is calculated. This result can be considered in good agreement with the experimental result of $1.4\times10^{10}\ s^{-1}$ if one takes into account the limits and simplifications of this theory in describing closely spaced large chromophores, as in the present case.[25] These findings confirm that, as in many other porphyrin noncovalent assemblies, energy transfer by the Förster mechanism is the most common mechanism. Whereas for covalently connected porphyrin arrays, when the connecting bridge is made of highly delocalized units (polyphenylethyne, oligo-phenylenevinylenes, etc.), the contribution to energy transfer by an electron-exchange (Dexter) mechanism[26] mediated by a superexchange[27] process has been reported,[28] this is almost never the case for self-assembled porphyrin arrays.[13] It is likely that close packing of the partners, and the nature of the weak interaction connecting them, favors the dipole–dipole interaction over the exchange interaction.

Conclusion

We have shown that at micromolar concentrations the coordination of **1** with a series of bidentate amines (DABCO, BIPY, and DPYP) induces the self-assembly of the components into a trigonal prismatic cage with the general formula $(diamine)_3$·**1**$_2$. Using optical absorption and ^{1}H NMR spectroscopy titrations, we have calculated the stability constants of the three cage assemblies. The molecular cages are destroyed in the presence of excess diamine to yield simple $(diamine)_3$·**1** open complexes. The double decker assembly with DPYP as the pillars is the less thermodynamically stable aggregate. The trigonal prismatic boxes prepared with photoactive **1** have been characterized from the spectroscopic and photophysical viewpoint. The assembly of the molecular subunits into cagelike aggregates induces spectral and photophysical changes in **1** when photochemically inert BIPY and DABCO are used as the pillars. However, when DPYP is used as the pillars of the molecular box, efficient photoinduced energy transfer (96%) occurs from the bases to the side walls. The rate of the energy-transfer process is in good agreement with that calculated by a dipole–dipole (Förster) mechanism after a correction for the orientation

factor that takes into account the unfavorable geometry of the donor–acceptor axial bond is introduced.

Experimental Section

The syntheses of Zn–TPPP[29] and **1**[16] have been previously reported. DPYP and MPYP were prepared and purified as described in the literature.[30]

^{1}H NMR spectra were recorded by using a Bruker Avance 500 Ultrashield NMR spectrometer. UV/Vis absorption spectra were measured by using a Shimadzu UV-2401PC spectrophotometer with 10 mm optical path cells except in the spectrophotometric titration of **1** with DPYP in which 1 mm optical path cells were employed. All solvents were of HPLC grade quality, obtained commercially, and used without further purification. The spectrophotometric titrations were carried out by running a spectrum of a solution of **1** in toluene at a concentration of around 10^{-6} M and adding incremental aliquots of the guest solution. Several guest solutions with different concentrations were used and after each addition a new UV/Vis spectrum was measured. Dilution of the host was avoided by preparing the guest solutions with the host solution in toluene as the solvent. The data obtained from the UV/Vis spectrophotometric titrations were analyzed by fitting the whole series of spectra at 1 nm interval by using the SPECFIT software,[18a] which uses a global system with expanded factor analysis and Marquardt least-squares minimization to obtain globally optimized parameters.

^{1}H NMR spectroscopy titrations were carried out by recording a spectrum of the MPYP solution in deuterated toluene at a concentration of 10^{-3} M and adding incremental aliquots of solution of **1** at a concentration of around 10^{-3} M. A new ^{1}H NMR spectrum was acquired after each addition. The solution of **1** was prepared by using the solution of MPYP in toluene as the solvent to avoid dilution.

The solvent used for photophysical determinations was spectroscopic grade toluene (C. Erba). DABCO (Aldrich) and BIPY (Merck) were used as received. Absorption spectra were recorded by using a Perkin–Elmer Lambda 9 spectrophotometer and emission spectra, uncorrected unless otherwise specified, were detected by using a Spex Fluorolog II spectrofluorimeter equipped with a Hamamatsu R928 photomultiplier. Luminescence quantum yields were evaluated from the area of the luminescence spectra, corrected for the photomultiplier response, with reference to TPP in aerated toluene ($\Phi_{fl}=0.11$).[31] Experiments at 77 K made use of quartz capillary tubes immersed in liquid nitrogen contained in a homemade quartz dewar. Absorption experiments were conducted in 5 mm optical path cells. Luminescence experiments were carried out on the same cells and the geometry used allowed excitation of a thin slice of solution at the edge of the cell from which the emission was collected to reduce reabsorption. Fluorescence lifetimes in the nanosecond range were detected by using IBH time-correlated single-photon counting apparatus with excitation at 560 nm. Luminescence lifetimes in the picosecond range were determined by using an apparatus based on an Nd:YAG laser (Continuum PY62–10) with a 35 ps pulse duration, 532 nm, 1.5 mJ per pulse, and a Streak Camera (Hamamtsu C1587 equipped with M1952). The luminescence signals from 1000 laser shots were averaged and the time profile was measured from the streak image in a wavelength range of approximately 20 nm around the selected wavelength. The overall time resolution of the system after the deconvolution procedure is 10 ps.[32]

Computation of the integral overlap and the rate for the energy-transfer processes according to the Förster mechanism were performed with the use of Matlab 5.2.[33] Molecular dimensions and distances were estimated with Chem 3D Ultra 6.0 software.[34] The minimized structure of the trigonal prismatic molecular box in Figure 5 was obtained with CAChe.[35] Estimated errors are 10% for lifetime values, 20% for quantum yields, and approximately 20% in the association constants. The working temperature, if not otherwise specified, was (295±2) K.

Acknowledgements

Financial support from Italian CNR (Project PM-P04–010 MACOL) and Ministero dell'Istruzione, dell'Universita' e della Ricerca (FIRB) as well as from Ministerio de Educación y Ciencia, SEUI, (CTQ2005–08989-C01-C02/BQU and CSD2006–0003), ICIQ Foundation and Generalitat de Catalunya (2005SGR00108) are grateful acknowledged. We thank COSTD31 for support.

[1] a) S. Bahatyrova, R. N. Frese, C. A. Siebert, J. D. Olsen, K. O. van der Werf, R. van Grondelle, R. A. Niederman, P. A. Bullough, C. Otto, C. N. Hunter, *Nature* **2004**, *430*, 1058–1062; b) G. McDermott, S. M. Prince, A. A. Freer, A. M. Hawthornwaite-Lawless, M. Z. Paziz, R. J. Codgell, N. W. Isaacs, *Nature* **1995**, *374*, 517–521; c) R. J. Codgell, N. W. Isaacs, A. A. Freer, J. Arrelano, T. D. Howard, M. Z. Paziz, A. M. Hawthornwaite-Lawless, S. M. Prince, *Prog. Biophys. Mol. Biol.* **1997**, *68*, 1–27; d) T. Pullerits, V. Sundström, *Acc. Chem. Res.* **1996**, *29*, 381–389.

[2] a) J. Deisenhofer, H. Michel, *Angew. Chem.* **1989**, *101*, 872–892; *Angew. Chem. Int. Ed. Engl.* **1989**, *28*, 829–847; b) R. Huber, *Angew. Chem.* **1989**, *101*, 849–871; *Angew. Chem. Int. Ed. Engl.* **1989**, *28*, 848–869.

[3] A. K. Burrell, D. L. Officer, P. G. Plieger, D. C. W. Reid, *Chem. Rev.* **2001**, *101*, 2751–2796.

[4] a) C. M. Drain, K. C. Russell, J.-M. Lehn, *Chem. Commun.* **1996**, 337–338; b) P. Ballester, R. M. Gomila, C. A. Hunter, A. S. H. King, L. J. Twyman, *Chem. Commun.* **2003**, 38–39; c) L. Baldini, P. Ballester, A. Casnati, R. M. Gomila, C. A. Hunter, F. Sansone, R. Ungaro, *J. Am. Chem. Soc.* **2003**, *125*, 14181–14189.

[5] a) M.-S. Choi, T. Yamazaki, I. Yamazaki, T. Aida, *Angew. Chem.* **2004**, *116*, 152–160; *Angew. Chem. Int. Ed.* **2004**, *43*, 150–158; b) R. Takahashi, Y. Kobuke, *J. Am. Chem. Soc.* **2003**, *125*, 2372–2373; c) Y. Kuroda, K. Sugou, K. Sasaki, *J. Am. Chem. Soc.* **2000**, *122*, 7833–7834; d) R. A. Haycock, A. Yartsev, U. Michelsen, V. Sundström, C. A. Hunter, *Angew. Chem.* **2000**, *112*, 3762–3765; *Angew. Chem. Int. Ed.* **2000**, *39*, 3616–3619; e) T. Hayashi, H. Ogoshi, *Chem. Soc. Rev.* **1997**, *26*, 355–364; f) O. Shoji, S. Okada, A. Satake, Y. Kobuke, *J. Am. Chem. Soc.* **2005**, *127*, 2201–2210; g) A. Satake, Y. Kobuke, *Tetrahedron* **2005**, *61*, 13–41.

[6] a) A. Prodi, C. Chiorboli, F. Scandola, E. Iengo, E. Alessio, R. Dobrawa, F. Würthner, *J. Am. Chem. Soc.* **2005**, *127*, 1454–1462; b) C. C. Mak, N. Bampos, S. L. Darling, M. Montalti, L. Prodi, J. K. M. Sanders, *J. Org. Chem.* **2001**, *66*, 4476–4486; c) E. Alessio, M. Macchi, S. Heath, L. G. Marzilli, *Chem. Commun.* **1996**, *12*, 1411–1412; d) M. S. Rodriguez-Morgade, T. Torres, C. Atienza-Castellanos, D. M. Guldi, *J. Am. Chem. Soc.* **2006**, *128*, 15145–15154.

[7] U. Michelsen, C. A. Hunter, *Angew. Chem.* **2000**, *112*, 780–783; *Angew. Chem. Int. Ed.* **2000**, *39*, 764–767.

[8] J. E. Redman, N. Feeder, S. J. Teat, J. K. M. Sanders, *Inorg. Chem.* **2001**, *40*, 2486–2499.

[9] a) B. G. Maiya, N. Bampos, A. A. Kumar, N. Feeder, J. K. M. Sanders, *New J. Chem.* **2001**, *25*, 797–800; b) L. Giribabu, A. A. Kumar, V. Neeraja, B. G. Maiya, *Angew. Chem.* **2001**, *113*, 3733–3736; *Angew. Chem. Int. Ed.* **2001**, *40*, 3621–3624.

[10] a) H. Yamaguchi, M. Kamachi, A. Harada, *Angew. Chem. Int. Ed.* **2000**, *39*, 3828–3831; b) D. R. Reddy, B. G. Maiya, *J. Phys. Chem. A* **2003**, *107*, 6326–6333.

[11] P. P. Kumar, B. G. Maiya, *New J. Chem.* **2003**, *27*, 619–625.

[12] a) I. P. Danks, I. O. Sutherland, C. H. Yap, *J. Chem. Soc. Perkin Trans. 1* **1990**, 421–422; b) H. L. Anderson, C. A. Hunter, M. N. Meah, J. K. M. Sanders, *J. Am. Chem. Soc.* **1990**, *112*, 5780–5789; c) H. L. Anderson, J. K. M. Sanders, *Angew. Chem.* **1990**, *102*, 1478–1480; *Angew. Chem. Int. Ed. Engl.* **1990**, *29*, 1400–1403; d) C. A. Hunter, C. M. R. Low, M. J. Packer, S. E. Spey, J. G. Vinter, M. O. Vysotsky, C. Zonta, *Angew. Chem.* **2001**, *113*, 2750–2754; *Angew. Chem. Int. Ed.* **2001**, *40*, 2678–2682; e) K. Ogawa, Y. Kobuke, *Angew. Chem.* **2000**, *112*, 4236–4239; *Angew. Chem. Int. Ed.* **2000**, *39*, 4070–4073; f) P. N. Taylor, H. L. Anderson, *J. Am. Chem. Soc.*

1999, *121*, 11538–11545; g) R. V. Slone, J. T. Hupp, *Inorg. Chem.* **1997**, *36*, 5422- 5423; h) M. R. Johnston, M. J. Gunter, R. N. Warrener, *Chem. Commun.* **1998**, 2739–2740; i) D. Jokic, C. Boudon, G. Pognon, M. Bonin, K. J. Schenk, M. Gross, J. Weiss, *Chem. Eur. J.* **2005**, *11*, 4199–4209; j) F. D'Souza, O. Ito, *Coord. Chem. Rev.* **2005**, *249*, 1410–1422; k) H. L. Anderson, *Inorg. Chem.* **1994**, *33*, 972–981.

[13] a) L. Flamigni, M. R. Johnston, L. Giribabu, *Chem. Eur. J.* **2002**, *8*, 3938–3947; b) L. Flamigni, M. R. Johnston, *New J. Chem.* **2001**, *25*, 1368–1370; c) L. Flamigni, A. M. Talarico, F. Barigelletti, M. R. Johnston, *Photochem. Photobiol. Sci.* **2002**, *1*, 190–197; d) E. Iengo, E. Zangrando, E. Alessio, J.-C. Chambron, V. Heitz, L. Flamigni, J.-P. Sauvage, *Chem. Eur. J.* **2003**, *9*, 5879–5887; e) L. Flamigni, A. M. Talarico, B. Ventura, R. Rein, N. Solladié, *Chem. Eur. J.* **2006**, 12, 701–712.

[14] a) H. Imahori, E. Yoshizawa, K. Yamada, K. Hagiwara, T. Okada, Y. Sakata, *J. Chem. Soc. Chem. Commun.* **1995**, 1133–1134; b) K. Yamada, H. Imahori, E. Yoshizawa, D. Goztola, M. R. Wasielewski, Y. Sakata, *Chem. Lett.* **1999**, 235–236; c) D. Sun, F. S. Tham, C. A. Reed, L. Chacker, M. Burgess, P. D. W. Boyd, *J. Am. Chem. Soc.* **2000**, *122*, 10704–10705; d) M. Dudiè, P. Lhoták, I. Stibor, H. Petøíèková, K. Lang, *New J. Chem.* **2004**, *28*, 85–90; e) H. Iwamoto, M. Yamaguchi, S. Hiura, Y. Fukazawa, *Heterocycles* **2004**, *63*, 2005–2011.

[15] a) A. Prodi, C. Chiorboli, F. Scandola, E. Iengo, E. Alessio, *ChemPhysChem* **2006**, *7*, 1514–1519; b) H. L. Anderson, *Chem. Commun.* **1999**, 2323–2330; c) J. L. Sessler, J. Jayawickramarajah, A. Gouloumis, T. Torres, D. M. Guldi, S. Maldonado, K. J. Stevenson, *Chem. Commun.*, **2005**, 1892–94; d) F. D'Souza, G. R. Deviprasad, M. E. Zandler, M. E. El-Khouly, M. Fujitsuka, O. Ito, *J. Phys. Chem. A* **2003**, *107*, 4801–4807.

[16] P. Ballester, A. I. Oliva, A. Costa, P. M. Deyà, A. Frontiera, R. M. Gomila, C. A. Hunter, *J. Am. Chem. Soc.* **2006**, *128*, 5560–5569.

[17] a) C. A. Hunter, J. K. M. Sanders, J. A. Stone, *Chem. Phys.* **1989**, *133*, 395–404; b) C. A. Hunter, M. N. Meah, J. K. M. Sanders, *J. Am. Chem. Soc.* **1990**, *112*, 5773–5780.

[18] a) SPECFIT 3.0.40, Spectrum Software Associates, Marlborough, MA (USA), **2007**; b) H. Gampp, M. Maeder, C. J. Meyer, A. D. Zuberbühler, *Talanta* **1985**, *32*, 95–101; c) H. Gampp, M. Maeder, C. J. Meyer, A. D. Zuberbühler, *Talanta* **1986**, *33*, 943–951.

[19] Data analysis took into account the value of the calculated microscopic constant for the interaction of DABCO with Zn–TPPP (see reference [16] for the data analysis in chloroform). The value measured in toluene was $K_m = 6.3 \times 10^4\,\text{M}^{-1}$, which was very similar to that obtained in chloroform.

[20] $K_{31} = 2.2 \times 10^{15}\,\text{M}^{-3}$ and $K_{32} = 8.0 \times 10^{27}\,\text{M}^{-4}$ in chloroform (see reference [16]).

[21] L. Flamigni, A. M. Talarico, B. Ventura, C. Sooambar, N. Solladié, *Eur. J. Inorg. Chem.* **2006**, 2155–2165.

[22] D. Gust, T. A. Moore, A. L. Moore, H. K. Kang, J. M. DeGraziano, P. A. Liddell, G. R. Seely, *J. Phys. Chem.* **1993**, *97*, 13637–13642.

[23] Th. Förster, *Discuss. Faraday Soc.* **1959**, *27*, 7–17.

[24] W. Van der Meer, G. Coker III, S. Y. S. Chen in *Resonance Energy Transfer Theory and Data*, VCH, New York, **1994**, pp. 55–83.

[25] K. F. Wong, B. Bagchi, P. J. Rossky, *J. Phys. Chem. A* **2004**, *108*, 5752–5763, and references therein.

[26] D. L. Dexter, *J. Chem. Phys.* **1953**, *21*, 836–850.

[27] H. M. McConnell, *J. Chem. Phys.* **1961**, *35*, 508–515.

[28] a) H. S. Cho, D. H. Jeong, M. C. Yoon, Y. H. Kim, Y. R. Kim, D. Kim, S. C. Jeoung, S. K. Kim, N. Aratani, H. Shinmori, A. Osuka, *J. Phys. Chem. A* **2001**, *105*, 4200–4210; b) S. I. Yang, J. Seth, T. Balasubramanian, D. Kim, J. S. Lindsey, D. Holten, D. F. Bocian, *J. Am. Chem. Soc.* **1999**, *121*, 4008–4018; c) K. Pettersson, A. Kyrychenko, E. Ronnow, T. Ljungdahl, J. Martensson, B. Albinsson, *J. Phys. Chem. A* **2006**, *110*, 310–318.

[29] P. Ballester, A. Costa, A. M. Castilla, P. M. Deyà, A. Frontera, R. M. Gomila, C. A. Hunter, *Chem. Eur. J.* **2005**, *11*, 2196–2206.

[30] E. Alessio, M. Macchi, S. L. Heat, L. G. Marzilli, *Inorg. Chem.* **1997**, *36*, 5614–5623.

[31] P. G. Seybold, M. Gouterman, *J. Mol. Spectrosc.* **1969**, *31*, 1–13.

[32] L. Flamigni, *J. Phys. Chem.* **1993**, *97*, 9566–9572.

[33] Matlab 5.2. The MathWorks Inc. Natik Ma (USA), **1998**.

[34] CS Chem 3D Ultra CambridgeSoft, Cambridge MA (USA), **2000**.

[35] CAChe WorkSystem Version 6.1.12.33, Fujitsu Limited (USA), **2004**.

Received: January 7, 2008
Published online: March 27, 2008

